Phototautomerism of *o*-nitrobenzyl compounds: *o*-quinonoid *aci*-nitro species studied by matrix isolation and DFT calculations †

Ian R. Dunkin,*[a] Jerzy Gębicki,[b] Mariusz Kiszka[a,b] and David Sanín-Leira[a]

[a] *Department of Pure and Applied Chemistry, University of Strathclyde, Thomas Graham Building, 295 Cathedral Street, Glasgow, UK G1 1XL*
[b] *Institute of Applied Radiation Research, Technical University (Politechnika), Żwirki 36, 90–924 Łódź, Poland*

Received (in Cambridge, UK) 30th November 2000, Accepted 31st May 2001
First published as an Advance Article on the web 25th June 2001

Photolyses of 2-nitrobenzyl methyl ether and 2-nitrotoluene with 254 nm light have been investigated in Ar and N_2 matrices at 12 K, and have been found to give *o*-quinonoid *aci*-nitro species as the primary photoproducts, along with other products. The *o*-quinonoid species have UV absorptions at relatively long wavelengths (λ_{max} at 385–430 nm) and undergo facile secondary photolysis when irradiated in these absorption bands. By means of this selective photolysis, fairly complete IR spectra of the *o*-quinonoids have been obtained. Comparison of the matrix IR spectra of these species with simulated spectra computed using density functional theory (DFT) has confirmed the identity of these reactive intermediates. Moreover, detailed analysis of the fit between the computed and experimental IR spectra has allowed the specific stereoisomers generated to be identified with reasonable confidence. Computations have also been made of the relative energies of the starting compounds, intermediate *o*-quinonoid isomers and the possible secondary products, together with the transition states connecting them. The results of these computations indicate that the observed stereoisomer of each of the *o*-quinonoid species cannot arise by photoinduced H-atom transfer followed by isomerizations on the electronic ground-state surfaces, since the energy barriers for reversion to starting compounds are substantially lower than those for the necessary isomerizations. It is therefore concluded that H-atom transfer and conformational interconversion occur in an electronic excited state.

Introduction

Photocleavage of *o*-nitrobenzyl derivatives

The *o*-nitrobenzyl group is well known to provide photocleavable protection for hydroxy compounds, such as alcohols (*cf.* **1**), phenols (*cf.* **2**) and carboxylic acids.[1,2] Similar methodology has also been applied to the protection of thiols[3] and, utilizing polymer-supported *o*-nitrophenylglycols, of aldehydes.[4] More recently, the potential of *o*-nitrobenzyl as a photocleavable protecting group for nitrogen in indoles, benzimidazole and 6-chlorouracil has been evaluated;[5] the *o*-nitrobenzyloxycarbonyl group has been examined for the photolabile protection of nucleoside 5′-hydroxy groups;[6] new photolabile protecting groups for nucleosides and nucleotides have been found in the 2-(2-nitrophenyl)ethoxycarbonyl and the 2-(2-nitrophenyl)-ethylsulfonyl groups;[7] and the photoinduced release of carbonyl compounds from *o*-nitroaryldioxolanes has been examined, as part of a study of the protection of pheromones.[8] In addition, reactive functional groups in modified oligonucleotides have been selectively revealed by 365 nm irradiation of the appropriate *o*-nitrobenzyl based protecting groups, thus providing an attractive way of introducing structural diversity into oligonucleotides.[9]

In most organic photocleavage reactions a small molecule, such as N_2 or CO_2, is eliminated as one of the fragments. In contrast, the photocleavage of *o*-nitrobenzyl derivatives results in two substantial fragments, both capable of bearing functionality. As a consequence, materials containing *o*-nitrobenzyl groups can be developed for a variety of applications. Examples are photocleavable polymers for use as resists,[10,11] photocleavable cryptands[12] and photocleavable DNA building blocks.[13,14] The same basic photochemistry has been applied to the cleavage of oligonucleotides from solid-phase supports,[15] the selective C-terminal cleavage of peptides bound to polyethyleneglycol,[16] and to various other cleavable linkages for solid-phase synthesis.[17–23] Furthermore, *o*-nitrobenzyl photocleavage has been utilized for the release of a variety of biologically active molecules from so-called 'caged' precursors. For example, a 2,4-dinitrobenzyl diglyceride has been synthesized as a means of photoactivating protein kinase C;[24] nitrobenzyl-based phosphoramide mustards have been developed as potential prodrugs for cancer therapy;[25] and nitrobenzyl quaternary ammonium derivatives of norbutyrylcholine have been assessed as photolabile inhibitors of butyrylcholinesterase.[26] Other interesting applications can readily be envisaged.

Mechanistic studies

***o*-Nitrobenzyl ethers.** The mechanism of the photocleavage of *o*-nitrobenzyl ethers has previously been studied by flash photolysis.[27,28] The results led to the postulate of the reaction pathways shown in Scheme 1. Flash photolysis of 2-nitrobenzyl 4-cyanophenyl ether (**2**) in acetonitrile led to the observation of three transient species. The first, with λ_{max} at 650 nm and with a lifetime of about 50 ps, was identified as the triplet excited state of the starting material. The second, with λ_{max} at 460 nm and a lifetime of about 1 ns, was identified as the triplet biradical **6**; while the third, which persisted beyond 10 ns, had λ_{max} at about 420 nm and was assigned the *o*-quinonoid structure **4**.[28] There has also been a mechanistic investigation of the photolytic release of glucose from 2-*O*-(2-nitrobenzyl)-D-glucose at pH 7 in aqueous sodium phosphate at 295 K; the reaction was monitored on the μs timescale by transient absorption of the *o*-quinonoid species at 406 nm.[29]

† Electronic supplementary information (ESI) available: Tables S1–S4 and Figs. S1 and S2. See http://www.rsc.org/suppdata/p2/b0/b009630j/

 DOI: 10.1039/b009630j

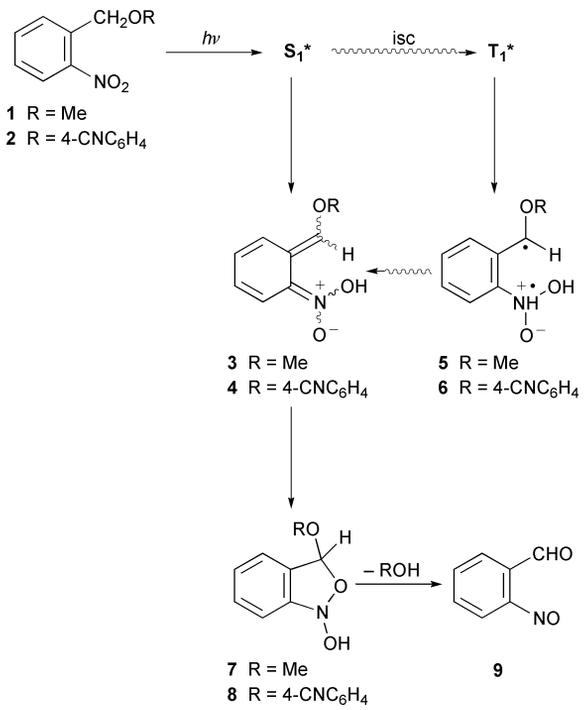

Scheme 1

o-Quinonoid molecules of this type—alternatively known as *aci*-nitro species—are assumed to be the primary ground-state intermediates in the photocleavage reactions of *o*-nitrobenzyl ethers and their analogues. They can arise either directly from the excited singlet states of their precursors or indirectly *via* the triplet manifold, as shown in Scheme 1. Under normal conditions in solution, the *o*-quinonoid species thus generated react further, supposedly *via* benzo[*c*]isoxazole intermediates (*cf.* **7** and **8**), yielding ultimately the unprotected hydroxy compounds and 2-nitrosobenzaldehyde (**9**). In most applications of the reaction, where the main aim is to recover or simply release the deprotected hydroxy compounds, the fate of the nitrosoaldehyde **9** is seldom determined. Nevertheless, **9** has been synthesized as a stable compound, by reduction of 2-nitrobenzaldehyde, and has been characterized by IR and visible absorption spectroscopy and by ^{1}H NMR.[30] The spectral data support the monomeric open structure **9** for this molecule.

***o*-Nitrobenzyl esters.** Besides the studies of *o*-nitrobenzyl ethers, flash photolysis investigations of several *o*-nitrobenzyl esters in polymer films between 77 and 473 K have also been carried out. These revealed two reaction pathways leading to the corresponding *o*-quinonoid intermediates: a very fast singlet route and a slower route *via* triplets.[31] The *o*-quinonoid intermediates had broad electronic absorptions with maxima at about 400 nm, and decayed non-exponentially with half-lives of about 100 μs at room temperature. The primary photoproducts from *o*-nitrobenzyl esters in various solutions have also been observed by time-resolved resonance Raman spectroscopy.[32]

More recently, the release of adenosine 5′-triphosphate (ATP) from its P^3-[1-(2-nitrophenyl)ethyl] ester, as well as the photolysis of a simpler methyl phosphate analogue, were investigated at pH 8.5 and 274 K by means of rapid scan FTIR and time-resolved, single-wavelength IR spectroscopy.[33] Transient IR bands due to the *o*-quinonoid intermediates were assigned with the aid of ^{13}C, ^{15}N and ^{18}O labelling. Under these conditions, however, the IR bands were fairly broad and the spectra were complicated by the presence of many functionalities in the molecules. Time-resolved monitoring showed that release of ATP occurred in a single exponential process, synchronous with the decay of the *o*-quinonoid species. The reactions of the by-product, 2-nitrosoacetophenone, with thiols were also investigated. In a further study, transient free radicals were observed, in addition to the *o*-quinonoid intermediate, following flash photolysis of the P^3-1-(2-nitrophenyl)ethyl ester of ATP in the presence of dithiothreitol.[34] The kinetics of formation of the radicals suggested that they arose by single-electron transfer to the triplet excited state of the nitroarene (*cf.* T_1* in Scheme 1), and it was proposed that they were radical anions of the nitroaryl group.

Related reactions. In studies of related photoinduced hydrogen-transfer reactions, a transient species with λ_{max} at about 440 nm was observed at low intensity following flash photolysis of 2-nitrobenzaldehyde,[35] and IR evidence that this was the *o*-quinonoid ketene **10** was derived from the photolysis of 2-nitrobenzaldehyde in argon matrices.[36] The ketene **10** (λ_{max} = 435 nm in Ar matrices) proved to be very photosensitive; so, despite careful selection of photolysis wavelengths, its IR bands were difficult to observe, and only weak ketene bands at 2118 and 2107 cm^{-1} could be detected. Notwithstanding the difficulties experienced in detecting **10** directly, its pK_a value (2.1) has been estimated from structural volume changes following photoexcitation of 2-nitrobenzaldehyde in aqueous solutions.[37]

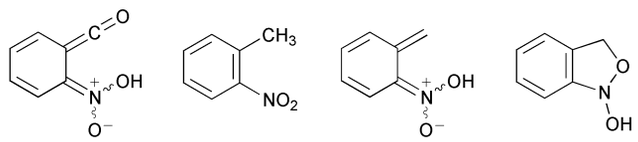

10 **11** **12** **13**

Finally, flash photolysis of 2-nitrotoluene (**11**) in aqueous solutions led to the detection of short-lived species with absorptions in the range 350–450 nm, which decayed with rate constants varying between 1 and 76 s^{-1} at 297 K.[38] The transient λ_{max} in these experiments was pH dependent; it was proposed that in acidic solution the predominant component was the *o*-quinonoid **12**, with a relatively short wavelength absorption (λ_{max} ~370 nm), while in alkaline solution the anion of **12** (λ_{max} ~420 nm) predominated. In spite of these observations, later attempts to observe the *o*-quinonoid **12** in Ar matrices, following UV irradiation of 2-nitrotoluene (**11**), were apparently unsuccessful.[39] This failure was attributed to rapid reversion of **12** to **11**. In the same study, a neutral species containing a hydroxy group [ν(OH) at 3526 cm^{-1}] was observed to arise from radical cations generated by X-ray radiolysis of matrix-isolated **11**, but the possibility that this species might have been the *o*-quinonoid **12** was rejected in view of the previously presumed readiness of **12** to revert to **11**. Results reported in this paper (see below) suggest that this conclusion could now be revised.

Objectives of this work. In view of the long-term and widespread interest in the photocleavage reactions of *o*-nitrobenzyl derivatives and their obvious potential for developing novel 'photochemical effect' materials with diverse applications, mechanistic studies of the reactions have been surprisingly few. For the most typical reactions of this class, *i.e.*, the cleavage of *o*-nitrobenzyl ethers or esters, there were apparently no investigations of the reactive intermediates by IR spectroscopy until 1997, when the time-resolved study carried out by Barth *et al.*[33] and a preliminary report of part of our own work[40] were published. Our main objectives in carrying out matrix-isolation investigations were to obtain IR spectra of examples of the *o*-quinonoid intermediates and thereby to determine their structures as fully as possible.

The matrix-isolation technique is particularly attractive as a method for characterizing reactive intermediates in photolyses. Firstly, owing to the lack of solvent absorptions in typical matrices such as Ar and N_2, more complete IR spectra of the various intermediates and products should be obtainable than

in, *e.g.*, polymer films, organic glasses or more normal solvents. Secondly, because of the narrow bandwidths and lack of rotational fine structure in typical matrix IR spectra, overlap of bands is minimized. This, in conjunction with the relatively small deviation from gas-phase values of matrix IR frequencies, facilitates comparison between observed and computed vibrational transitions. Finally, the matrix-isolation technique in conjunction with selective photolysis can be used to study the reactions of isolated molecules in a 'step-by-step' fashion, and thus help to establish reaction pathways.

In this paper we make a full report of our studies of the photolysis of 2-nitrobenzyl methyl ether (**1**) and 2-nitrotoluene (**11**) in Ar and N_2 matrices at 12 K. The work made use of both UV–visible and IR absorption spectroscopy, together with comparisons of the matrix IR spectra of the *o*-quinonoid intermediates with simulated spectra computed using density functional theory (DFT). We have also computed the energies of the starting compounds and the various other electronic ground-state species and transition states which could be involved in the reactions.

Results and discussion

Matrix photolysis of 2-nitrobenzyl methyl ether (1)

2-Nitrobenzyl methyl ether (**1**) was chosen for study, because it is the simplest 2-nitrobenzyl ether, and should therefore provide matrix photoproduct IR spectra with the fewest complications. In order to ascertain the electronic absorption characteristics of the starting material and any detectable photoproducts, investigation of the matrix photochemistry of **1** was first carried out with UV–visible absorption spectroscopy as the monitoring technique.

UV–visible absorptions. Fig. 1 shows UV–visible spectra of **1** in an Ar matrix, before and after 254 and 460 nm photolysis. A weak broad absorption with $\lambda_{max} = 430$ nm arose during the initial photolysis at 254 nm, and was bleached by subsequent irradiation at 430 or 460 nm. Very similar results were obtained with N_2 matrices. Allowing for differences in temperature, medium and starting material, the bleachable 430 nm absorption is very close to that of the long-lived intermediate observed after flash photolysis of the 4-cyanophenyl ether **2** (λ_{max} = 420 nm),[28] which was assigned the *o*-quinonoid structure **4**. On this basis, together with IR data which are discussed below, we identify the matrix-isolated photolabile intermediate with the 430 nm absorption as the *o*-quinonoid species, 5-methoxymethylene-6-*aci*-nitrocyclohexa-1,3-diene (**3**). In these matrix experiments, no absorption appeared at longer wavelengths that could be attributed to the triplet biradical **5**. This is not surprising, since it is unlikely that the matrix would prolong the lifetime of such a triplet species sufficiently for detection by normal spectroscopy.

IR absorptions. Table 1 lists the observed IR absorptions of **1** isolated in Ar and N_2 matrices. There is good agreement between the spectra for the two different matrix hosts, small differences in band positions and intensities being attributed to matrix site effects. Assignments have been made by reference to tabulations of group-frequency data.[41] All these bands diminished in intensity at comparable rates when the matrices were irradiated with 254 nm light, while a large number of new bands arose. Amongst the latter were absorptions which could be attributed to the expected final product, 2-nitrosobenzaldehyde (**9**) [ν(C=O) at 1724 (Ar) or 1719 (N_2), ν(NO) at 1527 (Ar) or 1528 cm^{-1} (N_2)].[30] The overall reaction thus appeared to follow the normal course, but clearly several product species were present.

Amongst the IR bands which arose on initial photolysis at 254 nm were a group which also diminished in intensity on subsequent long wavelength photolysis (430 ± 10 or 460 ± 10 nm). These latter IR bands behaved in exactly the same way as the broad electronic absorption at 430 nm, and are therefore assigned to the same intermediate species **3**. Fig. 2(a) is a portion of an IR difference spectrum showing the bands which diminished on 460 nm photolysis. Table 2 lists all the IR bands assigned to this intermediate in both Ar and N_2 matrices. There is excellent agreement between the two matrix hosts. In most experiments, irradiation at 460 nm (rather than 430 nm) was chosen so as to minimize further photolysis of the starting material. Even so, photolysis of **1** occurred to a small extent, as shown by the appearance of the strongest two IR bands of **1** as weak bands in the difference spectrum [Fig. 2(a)].

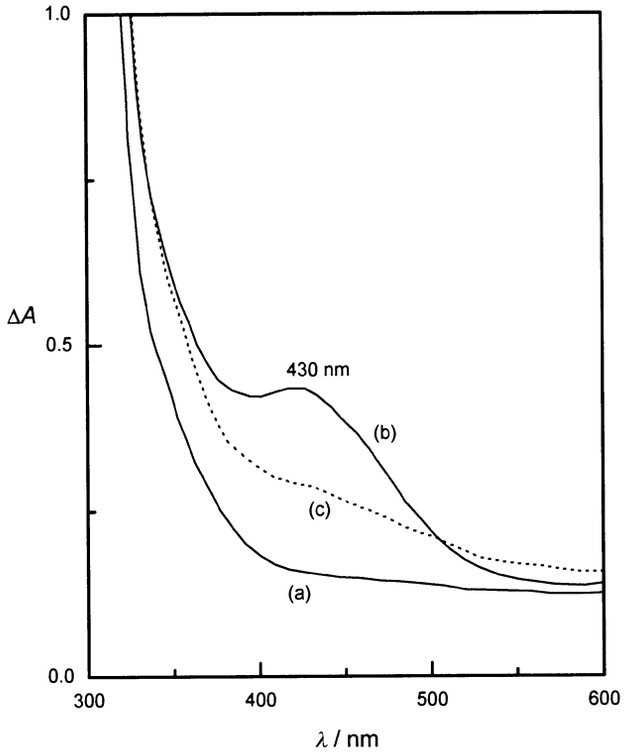

Fig. 1 UV–visible absorption spectra of 2-nitrobenzyl methyl ether (**1**) in an Ar matrix at 12 K: (a) before photolysis; (b) after 6.5 min photolysis at 254 nm; (c) after a further 30 min photolysis at 460 ± 10 nm. The spectra all have the background subtracted.

Identification and stereochemistry of 3. The observed IR absorptions of the photolabile intermediate generated from **1** are not easily assigned to particular structural features. In the preliminary report of our investigation,[40] we attributed these absorptions to the *o*-quinonoid species **3** solely through assigning some of the more prominent bands by comparison with tabulations of group frequencies for ethers, nitrones and oximes.[41–43] Nevertheless, apart from the OH group, the functionality in **3** gives rise to IR bands only in the skeletal region of the spectrum, where assignments are difficult to make with certainty. Thus, although there was no qualitative discrepancy between expectation and observation, a more rigorous interpretation of the IR spectrum was desirable.

There were two issues to be settled with regard to the matrix-isolated intermediate observed after photolysis of 2-nitrobenzyl methyl ether (**1**): firstly to confirm its identity as the *o*-quinonoid species **3**, and secondly to ascertain its stereochemistry if possible. In principle, **3** could exist as any of the four geometric isomers shown in Fig. 3 (*EE*, *EZ*, *ZE* or *ZZ*). For each of these geometric isomers, different conformers can arise from rotation of the OH group about the N–O bond (OH rotamers) and also from rotations of the methoxy group.

We have carried out DFT computations of the equilibrium geometries and IR transitions of all the isomers and conformations of **3** shown in Fig. 3, using the B3PW91 hybrid functional

Table 1 IR absorptions (cm^{-1}) of the starting materials, 2-nitrobenzyl methyl ether (**1**) and 2-nitrotoluene (**11**), isolated in Ar and N_2 matrices at 12 K

2-Nitrobenzyl methyl ether (**1**)		2-Nitrotoluene (**11**)		Assignment
Ar matrix	N_2 matrix	Ar matrix	N_2 matrix	
3093 vw[a]	3093 vw	3072[a]	3073	ν(CH) aromatic
2998	3002			
2935	2938	2999	3000	ν(CH) side chain
2911	2915	2994	2945	
2890	2896	2876	2878	
2830	2830			
2090 vw	2090 vw			Combination band
1870 vw	1874 vw			Combination band
1618	1617	1618 s	1617 s	ν(C=C) aromatic
	1598			
1581 vw	1581 vw	1584 m	1583 m	
1535 vs	1536 vs	1534 vs	1535 vs	$\nu_a(NO_2)$
1469	1481	1486	1486	ν(C=C) aromatic
1452	1454	1463	1465	
		1444		
		1432	1432	
1378 m	1382	1386	1386	
1344 s	1351 s	1352 vs	1355 vs	$\nu_s(NO_2)$
1309	1303 vw	1308 m	1308 m	
1203 m	1204			
1120 s	1116 s			ν_a(C–O–C)
1078	1079			
983 m	981 m			
933 vw	932 vw			
860	859	860 s	860 s	
792	796	789 m	790 m	
728 m	734 m	728 s	732 s	γ(CH)aromatic
684	684	689	692	
		667	667	

[a] Bands were weak unless denoted vs (very strong), s (strong), m (medium), or vw (very weak).

in conjunction with the 6-31G(d) basis set.‡ This involved a thorough study of the OH rotamers, but we did not consider separately all the possible conformers that could arise from rotations of the methoxy group. For two of the conformations (*anti-EE*- and *anti-ZE*-**3**) no local energy minima could be located. Selected computed data for each of the remaining six isomers are given in Fig. 3. The computed IR transitions for these six isomers in the region 1800–500 cm^{-1} are presented in Fig. 2 for visual comparison with the experimental argon-matrix spectrum. The computed IR transitions of *syn-EE*- and *syn-EZ*-**3** in the region 4000–700 cm^{-1} are listed in Table 2.§

The fit between the experimental IR spectrum assigned to **3** and that computed for *syn-EE*-**3** is remarkably good with regard to both frequencies and relative band intensities. The frequencies of all the observed bands lie within 2% of their most plausible counterparts in the calculated spectrum, except for the band at 740 (Ar) or 746 cm^{-1} (N_2), which has a discrepancy of up to 2.6%. Moreover, there is a good correlation between calculated and observed band intensities; and no predicted band with an intensity >7% relative to that of the most intense absorption is missing from the experimentally accessible regions of the spectrum, except for those at 1649 and 1627 cm^{-1}, which overlap with the broad absorption of a secondary product. The computed spectrum for *syn-EZ*-**3** might also be regarded as a satisfactory match with experiment, though the fit is not as good as for *syn-EE*-**3**, but the computed spectra for the other four isomers are all poor matches with experiment.

‡ The performance of various functionals in combination with the 6-31G(d) basis set in predicting vibrational frequencies has been the subject of an extensive study.[44] From this, the B3PW91 hybrid functional appears marginally superior to the more commonly encountered B3LYP hybrid.[45]

§ Complete DFT IR data for all six of the identified stable conformations of **3** are provided as ESI (Table S1).

In comparing the spectra of *syn-EE*-**3** [Fig. 2(b)] and *syn-EZ*-**3** [Fig. 2(c)] with the experimental spectrum of **3** [negative bands in Fig. 2(a)], the following points are noteworthy. There are no obvious negative bands between 1600 and 1700 cm^{-1} in the experimental spectrum; *syn-EE*-**3** is predicted to have two relatively weak bands in this region, which would overlap with the broad secondary product absorption at 1637 cm^{-1}, whilst *syn-EZ*-**3** is predicted to have significantly stronger bands in similar positions, which might be expected to have been detectable, despite the overlap. The experimental band at 1384 cm^{-1} is well reproduced in the computed spectrum for *syn-EE*-**3** but not in that for the *syn-EZ* isomer. Band frequencies and relative intensities for the strongest experimental absorption at 1244 cm^{-1} and it weaker neighbour at 1267 cm^{-1} and also for the group of four weak bands between 1101 and 1205 cm^{-1} are all better matched by the *syn-EE* predictions. Similarly, the four experimental bands at frequencies below 1000 cm^{-1} are matched closely in the computed *syn-EE* spectrum, but much less satisfactorily in that of the *syn-EZ* isomer.

Therefore, detailed comparison of the argon-matrix IR spectrum assigned to **3** with the computed spectra for the various possible isomers (see both Fig. 2 and Table 2) confirms the identity of the matrix-isolated intermediate as the postulated *o*-quinonoid species, most probably trapped as the *syn-EE* isomer.

Secondary photolysis of 3. On photolysis with 460 nm light, the *o*-quinonoid intermediate **3** gave a new species (possibly more than one) with prominent IR bands at 1637, 1091 and 756 cm^{-1}, but no carbonyl band in the neighbourhood of 1700 cm^{-1}, and no obvious electronic absorption at $\lambda > 350$ nm (shorter wavelength absorptions would have been masked by other strong absorptions). This is consistent with the formation of the bicyclic intermediate **7**, in which the aromatic ring is

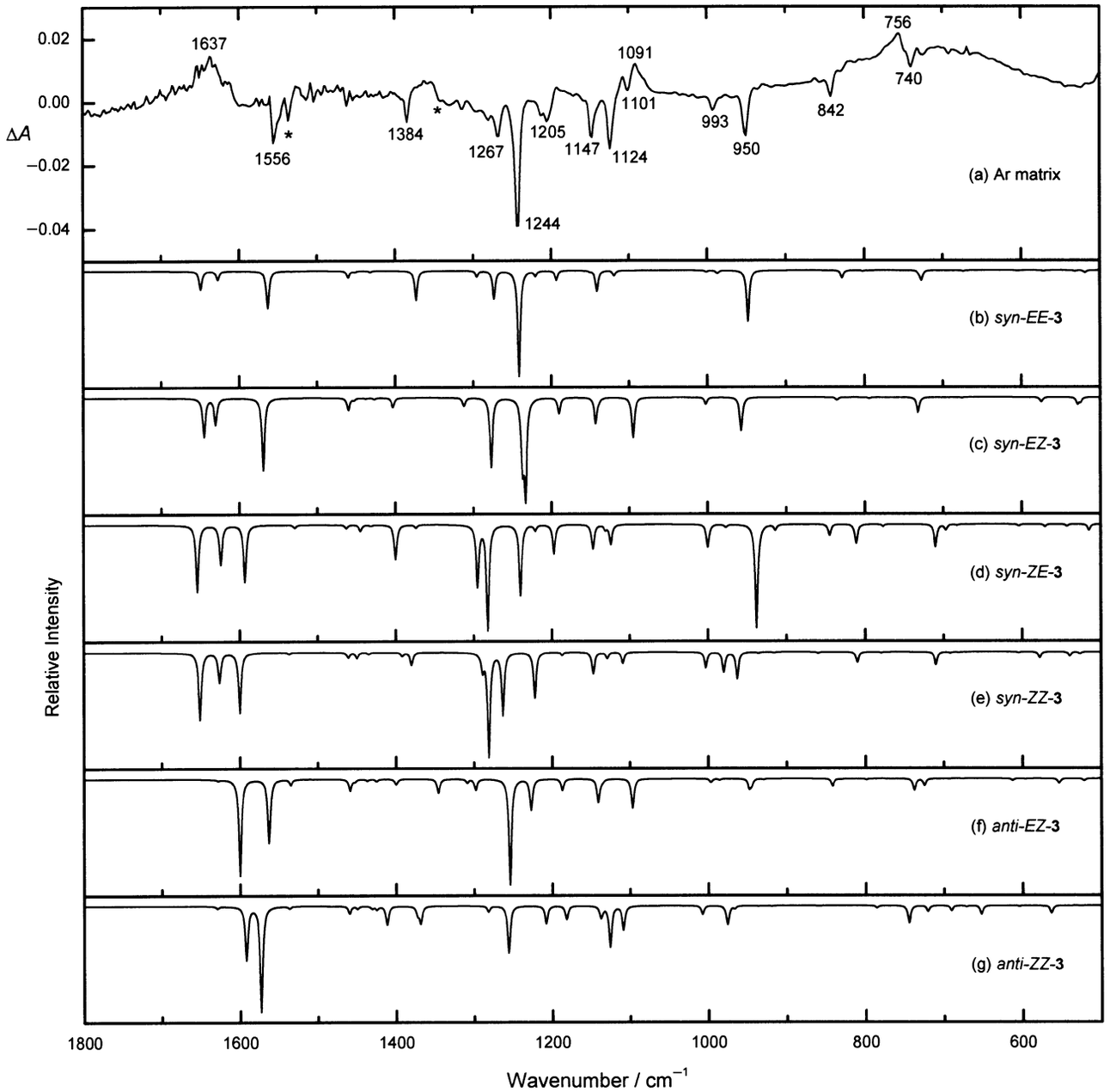

Fig. 2 IR spectra of the *o*-quinonoid intermediate **3** in the region 1800–500 cm^{-1}. (a) Difference spectrum obtained after 1.5 h photolysis of **1** in an Ar matrix at 12 K with 254 nm light, followed by 3 h photolysis at 460 ± 10 nm; absorptions which diminished on 460 nm photolysis are shown as negative bands (downwards) and are assigned to **3**, except for the two bands marked with asterisks, which are the strongest two bands of **1**. (b)–(g) Simulated IR spectra of stereoisomers of **3** (*cf*. Fig. 3); to assist visual comparison between the computed and experimental spectra, computed bands have been given a Lorentzian line shape with FWHM = 4 cm^{-1}.

regained. DFT calculations of the IR transitions of **7**¶ were also reasonably consistent with the three observed bands. Nevertheless, the photoinduced reaction of **3** in matrices will not necessarily be the same as its normal thermal reaction, and too few IR bands of the secondary photoproduct from **3** have been observed to allow its unequivocal identification, or even to decide whether only one secondary product is formed. Significant further photolysis of **7** would not occur at 460 nm; so that, when **3** was photolysed at 460 nm, no increase in intensity was expected for the IR bands attributed to nitrosobenzaldehyde **9**, and none was observed.

Matrix photolysis of 2-nitrotoluene (11)

During our investigation of the matrix photolysis of **1**, and once the need to calculate the IR transitions of **3** had become apparent, preliminary computations were carried out for the simpler *o*-quinonoid species **12**, which lacks the methoxy group present in **3** and therefore has fewer stereoisomers. In this context, we also decided to try generating **12** by matrix photolysis of 2-nitrotoluene (**11**), despite the reported failure of an earlier attempt.[39] It was felt that the key to observing this species in matrices might lie in the use of the monochromatic 254 nm light from a low-pressure mercury arc. We therefore carried out matrix-photolysis studies of **11**, similar to those described above for **1**. In view of our success in generating **12** (see below), the previously reported photostability of matrix-isolated **11** is puzzling.

UV–visible absorptions. Fig. 4 shows UV–visible spectra of **11** in an N_2 matrix, before and after 254 and 395 nm photolysis. A weak, broad absorption with λ_{max} = 385 nm arose during the initial photolysis at 254 nm, and was bleached by subsequent irradiation at 395 nm. A second photoproduct with λ_{max} =

¶ The results of these calculations are provided as ESI (Table S3).

Table 2 IR bands (cm^{-1}) assigned to *o*-quinonoid species **3**, arising after 254 nm photolysis of **1** in Ar and N_2 matrices at 12 K, and diminishing upon subsequent long wavelength photolysis (460 ± 10 nm); compared with calculated IR transitions in the 4000–700 cm^{-1} region for *syn-EE*- and *syn-EZ*-**3**[a]

Experimental		Calculated[b]		Assignment[c]
Ar matrix	N_2 matrix	*syn-EE*-**3**	*syn-EZ*-**3**	
3533 w[d]	3519 w[d]	3556 (23.8)	3533 (42.1)	ν(OH)
		3128 (0.8)	3138 (1.3)	ν(CH) exocyclic C=CH
		3126 (0.3)	3121 (1.1)	ν(CH) ring
		3102 (1.4)	3106 (1.9)	
		3080 (2.8)	3081 (4.4)	
		3067 (2.5)	3067 (4.4)	
		3044 (3.0)	3044 (4.6)	
		2984 (6.5)	2978 (11.0)	ν(CH) Me
2943 w	2946 w	2915 (18.1)	2911 (30.9)	
2115 w	2115 w			Combination band
		1649 (17.7)	1645 (41.7)	ν(C=N) + δ(NOH)
		1627 (8.4)	1630 (28.8)	ν(C=C) ring
	1587 w			
1556 s	1552 s	1563 (35.4)	1569 (77.8)	ν(C=C) exocyclic
		1533 (0.2)	1542 (0.2)	ν(C=C) ring
		1460 (6.5)	1460 (13.3)	δ(HCH) Me
		1452 (1.3)	1453 (2.1)	δ(HCH) Me
		1439 (0.2)	1438 (0.9)	
		1432 (1.3)	1427 (1.8)	
		1394 (0.1)	1403 (10.6)	
1384 m	1384 m	1373 (27.8)	1339 (0.2)	
		1295 (5.7)	1312 (9.3)	
1267 m	1270 s	1273 (26.6)	1277 (74.9)	δ(NOH)
			1237 (67.5)	$\nu(N^+–O^-)$ + δ(NOH)
1244 vs	1243 vs	1241 (100.0)	1233 (100.0)	ν(C–OMe) + δ(NOH)
		1220 (4.8)		$\nu(N^+–O^-)$ + δ(NOH) + δ(CH)
1205 m	1203 m	1193 (9.0)	1190 (17.1)	δ(CH)
		1150 (0.7)		
1147 s	1149 s	1141 (19.8)	1143 (27.9)	ρ(Me)
			1139 (2.1)	δ(CH) ring
		1134 (0.1)	1134 (0.1)	ρ(Me)
1124 s	1124 s	1119 (4.9)	1095 (43.0)	
1101 w	1098 m			
		1001 (1.4)	1002 (7.2)	
993 w	991 w	987 (2.9)	990 (0.2)	
950 s	956 s	948 (47.9)	957 (36.0)	δ(NOH) + ring deformation
		942 (<0.1)	945 (<0.1)	γ(CH) ring
		924 (<0.1)	928 (0.1)	γ(CH) ring
842 w	844 w	828 (7.3)	835 (3.2)	Ring deformation
		802 (0.8)	801 (0.2)	γ(CH) ring + exocyclic C=CH
		795 (0.3)	794 (1.2)	γ(CH) ring + exocyclic C=CH
		730 (1.7)		
740 w	746 w	727 (9.1)	732 (13.3)	γ(CH) ring
			731 (3.7)	

[a] The complete calculated IR data are available as electronic supplementary information (ESI, Table S1). [b] Calculated frequencies from B3PW91/6-31G(d) computations have been scaled by the standard factor of 0.9573 (refs. 42 and 43); computed band intensities relative to the strongest band at 1241 or 1233 cm^{-1} (100.0) are given in parentheses. [c] Assignments are approximate characterizations derived from the computed vibrational modes. [d] Experimental IR bands are denoted vs (very strong), s (strong), m (medium), w (weak), or vw (very weak).

275 nm was also formed in the initial 254 nm photolysis, but this did not undergo secondary photolysis with 395 nm light. Very similar results were obtained with Ar matrices. These observations accord with those obtained in a previous flash-photolysis study of **11** in aqueous solutions,[38] in which a transient intermediate with λ_{max} ~370 nm, identified as **12**, was observed, and in which an unidentified photostable product was also seen to accumulate. By analogy with the results for ether **1**, and from matrix IR data (see below), we identify the matrix-isolated photolabile species with the 385 nm absorption as the *o*-quinonoid, 5-methylene-6-*aci*-nitrocyclohexa-1,3-diene (**12**). Comparison of the electronic absorptions of **3** and **12** reveals a significant bathochromic shift (45 nm) due to the methoxy group in **3**. The second matrix photoproduct from **11**, with λ_{max} = 275 nm, remains unidentified.

IR absorptions. Table 1 lists the observed IR absorptions of **11** isolated in Ar and N_2 matrices. As with the ether **1**, there is good agreement between the spectra for the two different matrix hosts. All these bands diminished in intensity at comparable rates when the matrices were irradiated with 254 nm light, while many new bands arose. Amongst the latter were a group which diminished in intensity on subsequent long wavelength photolysis (395 ± 10 nm), thus behaving in exactly the same way as the 385 nm electronic absorption assigned to **12**. Fig. 5(a) is a portion of an IR difference spectrum showing the bands which diminished on 395 nm photolysis, and which are assigned to the *o*-quinonoid species **12**. Table 3 lists all the IR bands assigned to this intermediate in both Ar and N_2 matrices. There is excellent agreement between the two matrix hosts. The identification of **12** is supported by DFT computations of its IR transitions, as described below.

Identification and stereochemistry of 12. The *o*-quinonoid species **12** could exist in either the *E* or *Z* configuration (Fig. 6), with conformers arising from rotation of the OH group about the N–O bond. Equilibrium geometries, energies, vibrational frequencies and IR intensities were computed by the same DFT

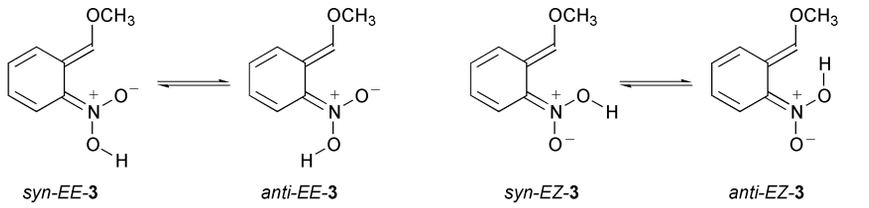

	syn-EE-**3**	*anti-EE*-**3**	*syn-EZ*-**3**	*anti-EZ*-**3**
Symmetry	C_s	—	C_s	C_1
θ_{NCCC} / °	0.0	—	0.0	20.4
θ_{ONOH} / °	0.0	—	0.0	146.0
ΔE / kJ mol^{-1}	0.0	—	17.6	46.7

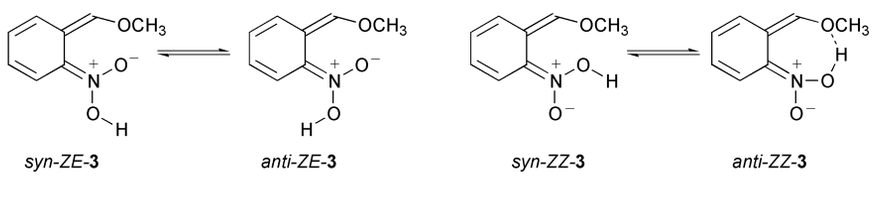

	syn-ZE-**3**	*anti-ZE*-**3**	*syn-ZZ*-**3**	*anti-ZZ*-**3**
Symmetry	C_1	—	C_1	C_1
θ_{NCCC} / °	30.6	—	33.5	29.3
θ_{ONOH} / °	2.9	—	0.5	137.4
ΔE / kJ mol^{-1}	30.0	—	39.4	37.4

Fig. 3 Geometrical isomers of **3** and conformations involving rotation about the N–OH bond. Computed data given for each isomer are the symmetry (point group) of the equilibrium geometry, the N=C–C=C (θ_{NCCC}) and O^-–N^+–O–H (θ_{ONOH}) dihedral angles and the energy relative to the most stable stereoisomer, *syn-EE*-**3**. No local energy minima were found for *anti-EE*- and *anti-ZE*-**3**.

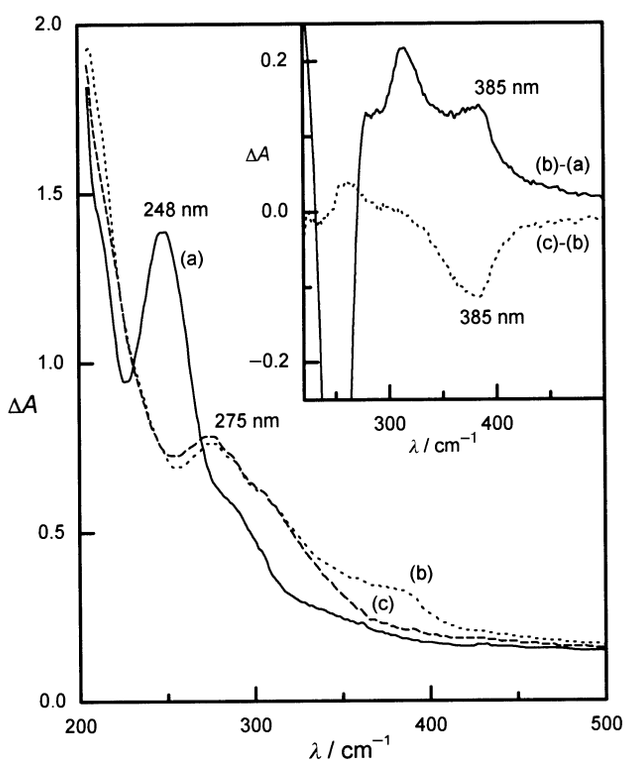

Fig. 4 UV–visible absorption spectra of 2-nitrotoluene (**11**) matrix-isolated in N_2 at 12 K: (a) before photolysis; (b) after 30 min photolysis at 254 nm; (c) after a further 30 min photolysis at 395 ± 10 nm. These spectra all have the background subtracted. The inset shows difference spectra, (b) − (a) and (c) − (b), showing the growth and disappearance, respectively, of a photolabile intermediate with λ_{max} = 385 nm.

methods used for **3** (see above). Fig. 6 includes selected computed data for *syn-E*-, *syn-Z*- and *anti-Z*-**12**; no local energy minimum was located for *anti-E*-**12**. Fig. 5 presents a comparison of the experimental IR spectrum assigned to **12** with the computed spectra. Table 3 includes the computed IR transitions for *syn-E*- and *syn-Z*-**12** in the region 4000–500 cm^{-1}.‖

Although our study of the photolysis of **11** was undertaken primarily to give a conformationally and spectroscopically simpler system than the photolysis of **1**, the IR spectrum of the primary photoproduct **12** [shown as negative peaks in Fig. 5(a)] ironically presents more difficulties for interpretation than the spectrum of its methoxy analogue **3**. The simulated spectrum for *syn-E*-**12** fits the experimental spectrum very well, except that, in the latter, there appear to be too many bands with significant intensity in the regions 1270–1150 and 1005–940 cm^{-1} [*cf.* Fig. 5(a) and (b)]. Apart from these extra bands, the experimental and computed spectra agree in frequency within 2.5% and there is also a good correlation between calculated and observed intensities. The fit between the experimental spectrum and that computed for *syn-Z*-**12** is significantly less good (*e.g.* frequency discrepancies up to 4%), whilst the computed spectrum for *anti-Z*-**12** is a very poor fit with experiment.

Close inspection of Fig. 5(a) reveals that some of the bands belonging to the primary photoproduct are appreciably broader than others, *e.g.* those at 979 and 947 cm^{-1}, suggesting the overlap of two or more absorptions. These broader bands and the presence of more bands than expected could be accounted for by matrix splittings. Such splittings can often be identified by comparison of IR spectra recorded with two different matrix hosts. Unfortunately, in our experiments with N_2 matrices, we obtained samples with poorer optical quality than the Ar matrices, in which it was difficult to identify the weaker IR bands. Thus, fewer IR bands of **12** are reported for N_2 than for Ar matrices (Table 3), and the identification of possible matrix splittings was thus frustrated. Notwithstanding the possibility

‖ Complete DFT IR data for all three of the identified stable conformations of **12** are provided as ESI (Tables S2 and S4).

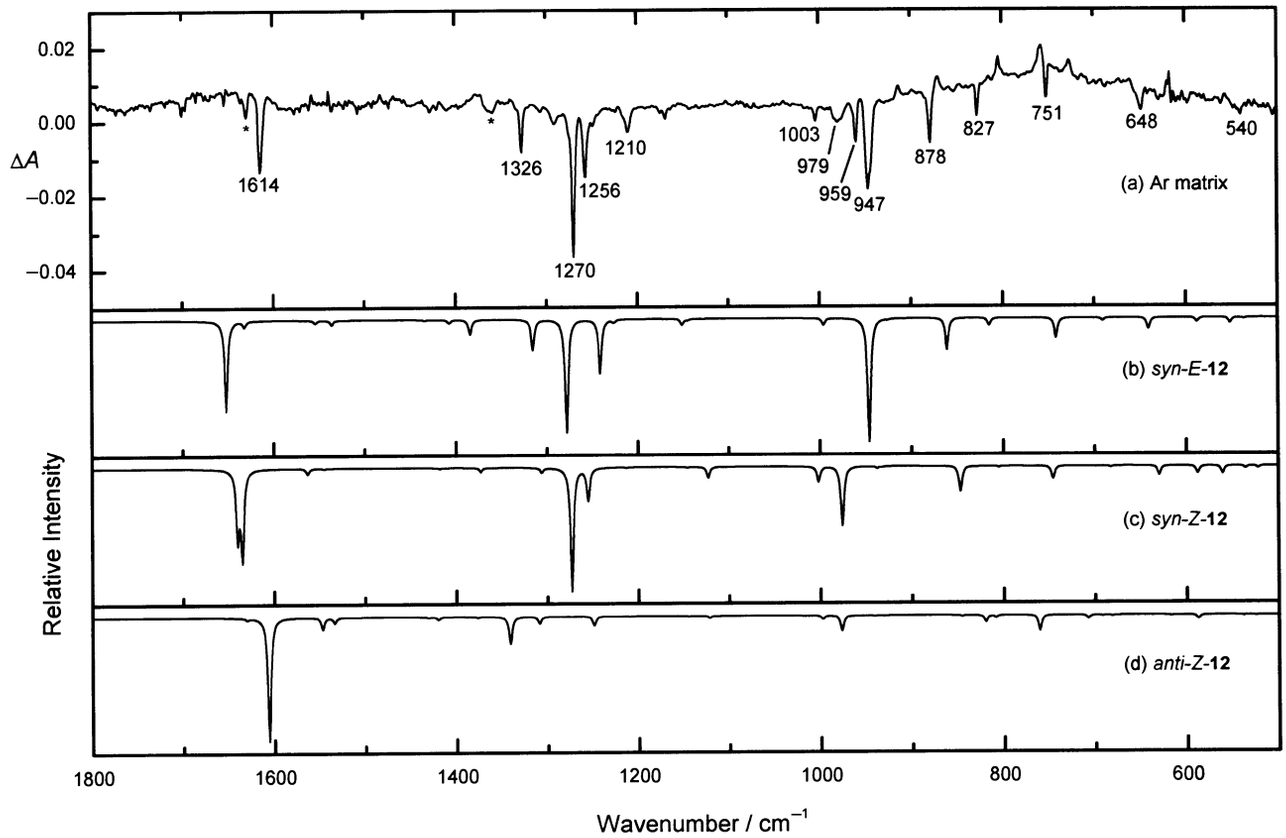

Fig. 5 IR spectra of the *o*-quinonoid intermediate **12** in the region 1800–500 cm^{-1}. (a) Difference spectrum obtained after 30 min photolysis of **11** in an Ar matrix at 12 K with 254 nm light, followed by 30 min photolysis at 395 ± 10 nm; absorptions which diminished on 395 nm photolysis are shown as negative bands (downwards) and are assigned to **12**. (b)–(d) Simulated IR spectra of stereoisomers of **12** (*cf.* Fig. 6); to assist visual comparison between the computed and experimental spectra, computed bands have been given a Lorentzian line shape with FWHM = 4 cm^{-1}.

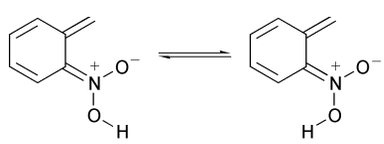

syn-E-**12** *anti-E*-**12**

Symmetry	C_s	—
θ_{NCCC} / °	0.0	—
θ_{ONOH} / °	0.0	—
ΔE / kJ mol^{-1}	0.0	—

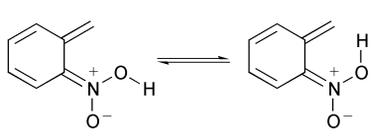

syn-Z-**12** *anti-Z*-**12**

Symmetry	C_s	C_1
θ_{NCCC} / °	0.0	20.6
θ_{ONOH} / °	0.0	159.9
ΔE / kJ mol^{-1}	12.2	32.7

Fig. 6 Geometrical isomers of **12** and conformations involving rotation about the N–OH bond. Computed data given for each isomer are the symmetry (point group) of the equilibrium geometry, the N=C–C=C (θ_{NCCC}) and O^-–N^+–O–H (θ_{ONOH}) dihedral angles and the energy relative to the most stable stereoisomer, *syn-E*-**12**. No local energy minimum was found for *anti-E*-**12**.

of matrix splittings, four factors suggest that at least two photolabile species were generated as primary photoproducts in the matrix photolysis of **11**: (i) the excellent fit between experimental and computed IR spectra for the more complex case of **3**, which was not paralleled in the case of **12**; (ii) the absence of any large matrix splittings for **3**, posing the question why there should be any for **12**; (iii) the magnitude of the separation between the IR bands in the two regions in question in Fig. 5(a), which are rather large for matrix splittings; and (iv) the variable bandwidths in the IR absorptions of Fig. 5(a). It should be noted that all the IR bands attributed to the primary photoproducts disappeared at comparable rates on photolysis with 395 nm light, and thus, if two or more species were generated as primary photoproducts, they had similar photoreactivity.

Without wishing to conclude too much from relatively minor observations, we suggest that the matrix photoproduct of **11** was either *syn-E*-**12** or a mixture of stereoisomers of **12** with the *syn-E* form predominating. In analogy with **3**, the secondary photolysis of **12** could have given rise to the benzoisoxazole **13**. Indeed, DFT computations of the IR transitions of this isoxazole** reproduced the pattern of weak positive-going bands in Fig. 5(a) rather well. Nevertheless, these experimental bands are too few and too weak to allow the identity of the secondary product or products to be firmly established.

The N–OH rotamers of 3 and 12

In nearly every case, the *syn* OH rotamers of **3** and **12** are predicted to have lower energy than the corresponding *anti* forms (see Figs. 3 and 6). Even so, the failure to find local

** Computed IR data for **13** are provided as ESI (Table S4).

Table 3 IR bands (cm^{-1}) assigned to *o*-quinonoid species **12**, arising after 254 nm photolysis of **11** in Ar and N_2 matrices at 12 K, and diminishing upon subsequent long wavelength photolysis (395 ± 10 nm); compared with calculated IR transitions in the 4000–500 cm^{-1} region for *syn-E*- and *syn-Z*-**12**[a]

Experimental		Calculated[b]		Assignment[c]
Ar matrix	N_2 matrix	*syn-E*-**12**	*syn-Z*-**12**	
	3521 w[c]			
3524 m[d]	3506 m	3548 (67.4)	3526 (58.4)	ν(OH)
	3481 w			
		3193 (1.2)	3194 (0.6)	ν(CH) C=CH_2
		3128 (1.0)	3121 (1.4)	
		3087 (9.1)	3087 (6.1)	ν(CH) ring
		3075 (10.3)	3076 (8.8)	
		3062 (0.4)	3064 (1.1)	ν(CH) ring + C=CH_2
		3055 (2.5)	3061 (0.6)	ν(CH) ring + C=CH_2
1614 s	1611 s	1652 (73.5)	1640 (53.6)	ν(C=N) + δ(NOH)
		1632 (5.0)	1635 (69.7)	ν(C=C) ring
		1554 (2.7)	1563 (4.6)	ν(C=C) exocyclic
		1536 (3.9)	1545 (0.6)	ν(C=C) ring
		1434 (0.7)	1431 (<0.1)	δ(CH)
		1407 (3.0)	1418 (0.9)	δ(CH) ring + C=CH_2
		1384 (12.0)	1373 (3.4)	
1326 m	1327 m	1315 (24.8)	1306 (4.0)	
1270 vs	1271 s	1278 (91.8)	1273 (100.0)	ν(N^+–O^- + δ(NOH)
1256 m		1241 (43.9)	1255 (26.5)	δ(NOH) + δ(CH)
1210 w		1226 (2.6)	1213 (0.5)	δ(CH)
		1151 (4.9)		δ(CH) ring
		1145 (1.1)	1146 (0.6)	δ(CH) ring + C=CH_2
			1123 (9.1)	δ(CH) ring + C=CH_2
1003 vw		996 (5.4)	1002 (12.4)	
979 w, br			976 (48.0)	ν(N–OH) + δ(CH)
959 m	959 w	947 (<0.1)	948 (0.1)	γ(CH) ring
947 s, br		946 (100.0)		ν(N–OH) + δ(CH)
		934 (0.2)	938 (1.4)	ρ(CH_2)
		926 (0.6)	933 (0.5)	γ(CH) ring
878 m	881 m	861 (25.8)	847 (20.4)	γ(CH) C=CH_2
827 m	828 m	815 (6.0)	829 (0.3)	Ring deformation
		804 (<0.1)	805 (0.8)	γ(CH)
751 m	755 w	742 (16.1)	746 (10.4)	γ(CH)
		701 (0.2)	699 (0.3)	
		691 (2.5)	683 (1.0)	
648 w	650 w	641 (9.0)	630 (7.4)	γ(CH) ring + C=CH_2
		588 (3.5)	588 (6.0)	δ(ONO) + ring deformation
540 vw		552 (4.4)	561 (6.1)	
		537 (0.9)	536 (2.1)	Ring deformation

[a] The complete calculated IR data are available as ESI (Table S2). [b] Calculated frequencies from B3PW91/6-31G(d) computations have been scaled by the standard factor of 0.9573 (refs. 42 and 43); computed band intensities relative to the strongest band at 946 or 1273 cm^{-1} (100.0) are given in parentheses. [c] Assignments are approximate characterizations derived from the computed vibrational modes. [d] Experimental IR bands are denoted vs (very strong), s (strong), m (medium), w (weak), or vw (very weak).

energy minima for *anti-EE*- and *anti-ZE*-**3** and for *anti-E*-**12** was surprising, especially since such local minima were found for the apparently more sterically congested *anti-EZ*- and *anti-ZZ*-**3** and *anti-Z*-**12**. The reason for this anomaly seems to lie in the ability of the molecules to twist well out of planarity about the C(5)–C(6) bond, to relieve steric strain in conformers like *anti-Z*-**12**; but similar twisting about C(6)–C(1) to relieve repulsions in, *e.g.*, *anti-E*-**12**, does not seem so favourable and the repulsions may be predominantly electrostatic (O···O) rather than steric. Moreover, *anti-ZZ*-**3**, which might be expected to be especially sterically crowded, is predicted to be stabilized by intramolecular H-bonding, and is thus the sole example of an *anti* form more stable than its *syn* rotamer.

Before we carried out the DFT calculations, we performed an extensive search of the conformation space of *E*- and *Z*-**12** and the N–OH rotamers of the four geometric isomers of **3**, utilizing AM1 and other semi-empirical methods. Plots of relative energies from the AM1 computations *versus* H–O–N^+–O^- dihedral angle†† are in good qualitative agreement with the DFT computations, particularly in predicting no local energy minima for *anti-EE*- and *anti-ZE*-**3** and for *anti-E*-**12**.

Reaction pathways

In the photolysis of **1** or **11**, when the transfer of a hydrogen atom takes place from the methylene or methyl group to the nitro group, the newly formed *aci*-nitro functionality might be expected to be generated initially in an *anti-Z* conformation. On this basis, the expected matrix-isolated primary photoproducts would be *anti-EZ*- or *anti-ZZ*-**3** from **1** and *anti-Z*-**12** from **11**. This raises the question of why the observed major primary photoproducts appear to be *syn-EE*-**3** and *syn-E*-**12**.

In an attempt to provide an answer to this question, and in addition to the calculations of structures and IR transitions for **3** and **12** described above, we have calculated optimized geometries and energies of the electronic ground states of both starting compounds (**1** and **11**), the possible secondary products **7** and **13**, and the transition states leading from the starting materials *via* the appropriate stereoisomers of **3** and **12** to these secondary products. The results of these computations are shown in Fig. 7.

The earlier flash-photolysis studies of **2** indicated that the

†† Provided as ESI (Figs. S1 and S2).

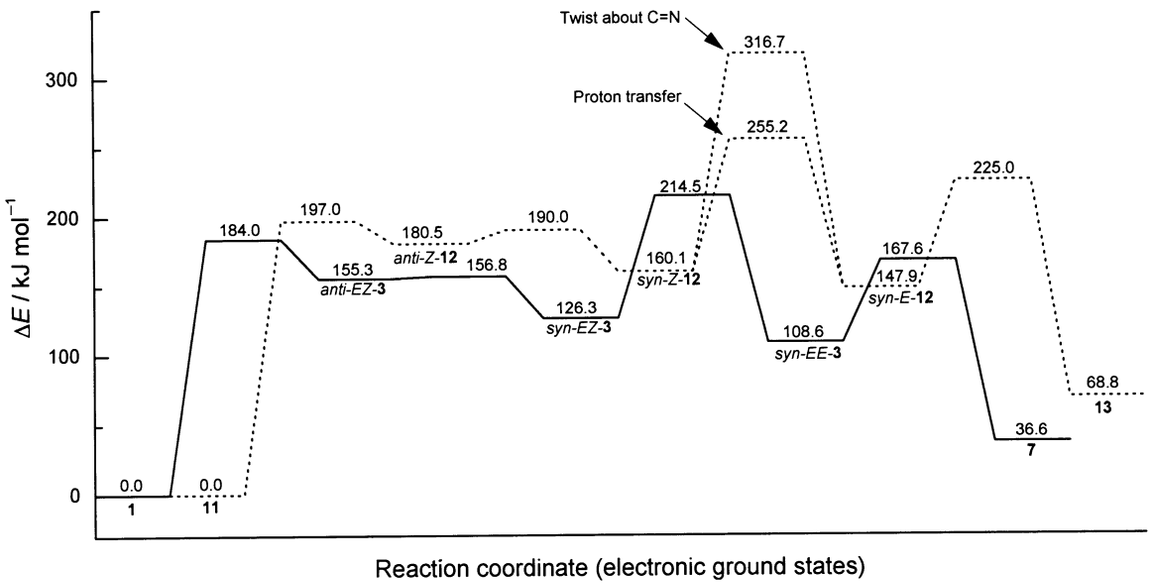

Fig. 7 Electronic ground-state energies, relative to the starting compounds, of the species, including transition states, which could be involved in the transformation of **1** *via* **3** to **7** (solid line) and of **11** *via* **12** to **13** (dotted line). For the conversion of *syn-Z*-**12** into *syn-E*-**12**, two transition states were examined: proton transfer from one O atom of the *aci*-nitro group to the other, and twisting of the *aci*-nitro group about the C=N bond. The energies were computed using the B3PW91/6-31G(d) model chemistry.

initial H-atom transfer to the nitro group occurs in a triplet excited state.[27,28] In the photolyses of **1** and **11**, this pathway would lead initially to triplet *anti-EZ*-**3** and *anti-Z*-**12**, respectively. Thereafter, configurational and conformational isomerism could, in principle, occur either on the triplet energy surface or *via* vibrationally excited electronic ground states.

Fig. 7 shows that, in the electronic ground states, both *anti-EZ*-**3** and *anti-Z*-**12** lie in shallow energy minima, with activation barriers leading to the corresponding more stable *syn* conformers of only 1.5 and 9.5 kJ mol^{-1}, respectively. Even the smaller of these barriers is quite large compared with *RT* at 12 K (0.1 kJ mol^{-1}), but the 254 nm photon, which initiates the photolysis and which has an energy equivalent to 470 kJ mol^{-1}, would provide ample excess vibrational energy in the primary photoproducts. Thus, it is not surprising that *anti-EZ*-**3** and *anti-Z*-**12** were not detected experimentally.

Fig. 7 also shows, however, that there are substantial energy barriers (over 95 kJ mol^{-1}) for the necessary $Z \rightarrow E$ isomerizations, *i.e.*, to convert *syn-EZ*-**3** and *syn-Z*-**12** into the major photoproducts actually observed—*syn-EE*-**3** and *syn-E*-**12**, respectively. Moreover, these barriers are larger than those for reversion to the corresponding starting compounds (57.7 and 36.9 kJ mol^{-1}). Therefore, if matrix photolysis of **1** and **11** proceeded by isomerization of *anti-EZ*-**3** and *anti-Z*-**12** in their vibrationally excited electronic ground states, we might expect *syn-EZ*-**3** and *syn-Z*-**12** to be trapped in the matrices, but not the *syn-EE* and *syn-E* forms, even though the latter are the most stable stereoisomers. It is true that the 254 nm photon which initiates the reaction could provide more than enough excess vibrational energy to surmount all the ground-state energy barriers depicted in Fig. 7, but reversion to the starting compounds would be the favoured reaction pathway for both **3** and **12**.

The $Z \rightarrow E$ isomerization required for the formation of the *E* configuration of the *aci*-nitro group in **3** or **12** could occur either by proton transfer from one oxygen atom of the *aci*-nitro group to the other or by twisting of the *aci*-nitro group about the carbon–nitrogen double bond. It seemed obvious that the proton transfer route would have the lower energy barrier, but we confirmed this in the case of the simpler system by computing the energies of both transition states for conversion of *syn-Z*-**12** into *syn-E*-**12** (see Fig. 7).

In view of the foregoing discussion, the observed products in the matrix photolyses of **1** and **11** are difficult to reconcile with isomerization processes occurring in the electronic ground sates. Assuming that our computations have provided reasonable estimates for the relative energies of all the species involved, we conclude that the isomerizations of **3** and **12** probably proceed *via* triplet excited states (*cf.* **5** and **6** in Scheme 1). Rotations about the carbon–nitrogen bond and the exocyclic carbon–carbon bond in these triplet species could have much lower energy barriers than in the singlet ground states, thus allowing the most stable geometrical isomers of the *o*-quinonoid species to be attained relatively easily. Once formed in their electronic ground states, the most stable isomers lie in relatively deep energy wells, with substantial barriers to reversion to the precursor molecules or cyclization to the presumed secondary products **7** and **13**.

The analogous photoenolizations of *o*-alkylphenyl ketones have been studied in detail,[46] and provide further well known examples of H-atom transfer between *ortho* aromatic substituents to give *o*-quinonoid species. In these reactions, H-atom transfer also typically occurs in the T_1 state of the excited ketone, to give the *o*-quinonoid photoenol initially as a triplet, which subsequently decays to the singlet ground-state photoenol. There is thus some similarity between the photochemistry of *o*-alkylphenyl ketones and *o*-nitrobenzyl compounds.

Finally, it should be noted that the reaction pathways discussed as possibilities for the matrix photolyses of **1** and **11** are appropriate for the reactions of isolated molecules, but will probably not apply to the equivalent solution-phase reactions, especially where protic solvents are utilized. In solution, proton transfer could be greatly assisted by intermolecular interactions between solvent and reactant or between two reactant molecules, thus lowering some of the energy barriers shown in Fig. 7.

Conclusions

Photolysis of 2-nitrobenzyl methyl ether (**1**) and 2-nitrotoluene (**11**) with 254 nm light in Ar and N_2 matrices at 12 K generates the corresponding *o*-quinonoid *aci*-nitro species, **3** and **12**, respectively as the primary photoproducts, along with other products. The *o*-quinonoid species have UV absorptions at relatively long wavelengths (λ_{max} at 430 and 385 nm) and undergo facile secondary photolysis when irradiated in these absorption bands. This selective secondary photolysis serves to distinguish the UV and, most importantly, IR absorptions of **3** and **12** from

those of other products, most of which are presumed to arise by secondary photolysis of **3** or **12**. We have thus obtained for the first time fairly complete IR spectra for examples of the *o*-quinonoid species postulated as intermediates in the photocleavage of *o*-nitrobenzyl derivatives.

Comparison of the matrix IR spectra obtained for **3** and **12** with simulated spectra computed using the B3PW91 hybrid functional in conjunction with the 6-31G(d) basis set confirms the identity of these reactive intermediates. Any doubts over the identification of **3**, which in our preliminary report depended solely on a qualitative interpretation of the matrix IR spectrum, have thus been removed. Moreover, detailed analysis of the fit between the computed and experimental IR spectra suggests that **3** is generated in its most stable *syn-EE* form and not the *anti-EZ* or *syn-EZ* forms which might have been expected. Similar analysis of the spectra for **12** suggests that a mixture of isomers may be generated in the matrices, but, as with **3**, the most stable conformer (*syn-E*) seems to predominate. The identities of the secondary photoproducts have not been firmly established, mainly owing to the detection of too few IR bands for reliable comparison with simulated spectra. Nevertheless, the small number of IR bands observed to arise in the long-wavelength photolyses of **3** and **12** are at least consistent with the formation of the benzo[*c*]isoxazol-1-ols **7** and **13**, as postulated from previous studies.

Computations have also been made of the relative energies of the starting compounds, intermediate *o*-quinonoid isomers and the possible secondary products **7** and **12**, together with the transition states connecting them. The results of these computations indicate that the most stable stereoisomers of **3** and **12**, which are those actually observed, cannot arise by photo-induced H-atom transfer followed by $Z \rightarrow E$ isomerizations on the electronic ground-state surfaces, even with the aid of excess vibrational energy from the original photoexcitation. The energy barriers for reversion to starting compounds are substantially lower than those for the necessary isomerizations. It is therefore concluded that H-atom transfer and $Z \rightarrow E$ isomerization occur in electronic excited states, eventually leading directly to the most stable ground-state geometries, *e.g. via* conical intersections. This conclusion accords well with results obtained in a previous flash-photolysis study of an analogous system.

Finally, it is clear that the application of DFT computations in this study has greatly assisted the interpretation of the experimental results. Firstly, we are able to derive stereochemical information about the reactive species of interest, which has been traditionally difficult to achieve in matrix-isolation studies. Secondly, we have gained some insight into the energetics of the process leading from the precursor to the first detected photoproduct, specifically that $Z \rightarrow E$ isomerization probably occurs in an excited state and not on the electronic ground-state surface.

Experimental

Matrix experiments

Materials. 2-Nitrobenzyl methyl ether **1** was prepared, as reported previously, by treatment of 2-nitrobenzyl alcohol (Aldrich, 97%) with dimethyl sulfate under phase-transfer catalysis.[47] At room temperature in acetonitrile **1** had $\lambda_{max} = 261$ nm ($\varepsilon = 5400$ dm^3 mol^{-1} cm^{-1}). 2-Nitrotoluene (>99%) was purchased from Aldrich and used without further purification. Research grade argon (≥99.9994%) and nitrogen (≥99.995%) were obtained from BOC Ltd.

Equipment. The matrix-isolation cold cell and its method of use have been described in detail previously.[48–50] It consisted of a 25 mm diameter spectroscopic window screwed into a nickel-plated copper holder, enclosed in a stainless steel vacuum shroud and cooled by an APD Cryogenics Displex model HC-2 closed-cycle helium refrigerator. The vacuum shroud was pumped to about 10^{-5} mbar by means of an Edwards Diffstak model 63–105M oil diffusion pump and was fitted with external spectroscopic windows and several inlet ports. Matrix temperatures were measured by means of a Chromel–Au–0.07 atom% Fe thermocouple attached to the cold window holder, and could be varied by means of a small resistance heater connected to the temperature controller. The base temperature of the cold cell was 12 K. A small secondary vacuum line was used to handle the matrix gases and control deposition rates *via* a fine control needle valve. For UV–visible spectra, the cell was fitted with quartz external windows and matrices were deposited on a CaF_2 cold window; for IR spectra, a CsBr cold window and KBr external windows were used.

UV–visible spectra were recorded at a resolution of 1 nm on a Shimadzu UV-250 instrument, with a double monochromator and with a sample compartment modified to accommodate the cold cell. IR spectra were recorded on a Bomem MB-100 FTIR spectrometer, fitted with a DTGS or MCT detector and interfaced *via* a DSP-100 fast Fourier transform card to a Viglen 25 MHz 386SX computer with a co-processor. IR spectra were run with resolutions of 1 or 4 cm^{-1} and were acquired and processed with Galactic Industries LabCalc software. Photolyses were carried out at 254 nm with unfiltered low-pressure Hg arcs (Vilber Lourmat, 2 × 4 W or 2 × 8 W), and at 395 ± 10, 430 ± 10 and 460 ± 10 nm with a high-pressure Hg arc (Oriel, 200 W) *via* a high-radiance grating monochromator (Applied Photophysics, f/3.4).

Matrix deposition. Neither of the starting materials was sufficiently volatile for the convenient preparation of matrix-gas mixtures by standard manometric methods. Ar and N_2 matrices containing **1** or **11** were therefore prepared by direct evaporation of the starting material from a glass side-arm onto the spectroscopic window cooled to 12 K, with simultaneous deposition of an excess of the host gas. In these circumstances matrix host : guest ratios could not be determined but, judging by the narrow bands and lack of excessive matrix splittings in the IR spectra of the resulting matrices, adequate isolation seems to have been achieved. In all cases, a thin layer of the pure host gas was deposited before evaporation of the guest species began, and a similar layer was laid down at the end of the deposition process. For IR experiments, matrix deposition was continued until the strongest bands in the IR spectrum had an absorbance value of at least 1.0; typically this took 60–80 minutes. For UV–visible experiments, deposition times were considerably shorter.

Computations

DFT calculations using the B3PW91 hybrid functional and the 6-31G(d) basis set were carried out for both **3** and **12** by means of Gaussian 98W (Revisions A.7 and A.9)[51] on 333 MHz Pentium II and 800 MHz Pentium III PCs, both with 256 Mb of RAM. In these DFT calculations[45] optimized equilibrium geometries, energies, vibrational frequencies and IR band intensities were determined for the *syn* and *anti* conformations of the four geometric isomers of **3** and both geometric isomers of **12**. ‡‡ Geometry optimizations were carried out for each structure from several different non-planar (C_1) starting geometries. In particular, starting geometries with different values of θ_{ONOH} were adopted. Optimized geometries and energies were also computed for the two starting compounds, **1** and **11**, and the two benzoisoxazoles, **7** and **13**, which are the most likely secondary products. In addition, IR transitions were computed for **7** and **13**. §§ Spartan Pro v1.0.3 (Wavefunction, Inc.) and

‡‡ Computed IR data not included in Tables 2 and 3 are given as ESI.
§§ These results are provided as ESI (Tables S3 and S4).

GaussView v2.1 were used as graphic interfaces for the Gaussian 98W program; structures were transferred between Spartan Pro and Gaussian 98W in Brookhaven data format (.pdb).

Transition states were located by the STQN method,[52,53] using the optimized equilibrium geometries of the reactants and products as inputs. For each transition state, a frequency calculation was carried out to confirm that a true saddle point had been located and that the atomic motions associated with the single imaginary frequency were plausible for the reaction concerned.

Acknowledgements

We thank the University of Strathclyde and the Technical Univesity of Łódź for an exchange scholarship for MK, the EPSRC and the Royal Academy of Engineering for a research fellowship for IRD, and the EPSRC for equipment grants (GR/H29018 and GR/L61972).

References

1 R. W. Binkley and T. W. Flechtner, in *Synthetic Organic Photochemistry*, ed. W. M. Horspool, Plenum, New York, 1984, Ch. 7, pp. 375–423.
2 D. Döpp, in *CRC Handbook of Organic Photochemistry and Photobiology*, ed. W. M. Horspool and P.-S. Song, CRC Press, Boca Raton, Florida, 1995, Ch. 81, pp. 1019–1062.
3 V. N. Rajasekharan Pillai, in *CRC Handbook of Organic Photochemistry and Photobiology*, ed. W. M. Horspool and P.-S. Song, CRC Press, Boca Raton, Florida, 1995, Ch. 62, pp. 766–774.
4 M. J. Aurell, C. Boix, M. L. Ceita, C. Llopis, A. Tortajada and R. Mestres, *J. Chem. Res. (S)*, 1995, 452; M. J. Aurell, C. Boix, M. L. Ceita, C. Llopis, A. Tortajada and R. Mestres, *J. Chem. Res. (M)*, 1995, 2569.
5 T. Voelker, T. Ewell, J. Joo and E. D. Edstrom, *Tetrahedron Lett.*, 1998, **39**, 359.
6 A. Hasan, K.-P. Stengele, H. Giegrich, P. Cornwell, K. R. Isham, R. A. Sachleben, W. Pfleiderer and R. S. Foote, *Tetrahedron*, 1997, **53**, 4247.
7 H. Giegrich, S. Eisele-Bühler, C. Hermann, E. Kvasyuk, R. Charubala and W. Pfleiderer, *Nucleosides Nucleotides*, 1998, **17**, 1987.
8 L. Ceita, R. Mestres and A. Tortajada, *Bol. Soc. Quim. Peru*, 1998, **64**, 55; L. Ceita, R. Mestres and A. Tortajada, *Chem. Abstr.*, 1998, **129**, 189138x.
9 J. D. Kahl and M. M. Greenberg, *J. Am. Chem. Soc.*, 1999, **121**, 597.
10 A. Reiser, *Photoreactive Polymers*, Wiley, New York, 1989.
11 K. Feng, T. Matsumoto and T. Kurosaki, *Chem. Mater.*, 1997, **9**, 1362.
12 R. Warmuth, E. Grell, J.-M. Lehn, J. W. Bats and G. Quinkert, *Helv. Chim. Acta*, 1991, **74**, 671.
13 P. A. Wender, C. K. Zercher, S. Beckham and E.-M. Haubold, *J. Org. Chem.*, 1993, **58**, 5867.
14 P. Ordoukhanian and J.-S. Taylor, *J. Am. Chem. Soc.*, 1995, **117**, 9570.
15 M. M. Greenberg and J. L. Gilmore, *J. Org. Chem.*, 1994, **59**, 746.
16 A. Ajayaghosh and V. N. R. Pillai, *Tetrahedron Lett.*, 1996, **37**, 6421.
17 R. Rodebaugh, B. Fraser-Reid and H. M. Geysen, *Tetrahedron Lett.*, 1997, **38**, 7653.
18 E. B. Åkerblom, A. S. Nygren and K. H. Agback, *Molecular Diversity*, 1997–1998, **3**, 137.
19 E. B. Åkerblom, *Molecular Diversity*, 1999, **4**, 53.
20 D. L. McMinn, R. Hirsch and M. M. Greenberg, *Tetrahedron Lett.*, 1998, **39**, 4155.
21 K. C. Nicolaou, N. Watanabe, J. Li, J. Pastor and N. Winssinger, *Angew. Chem., Int. Ed.*, 1998, **37**, 1559; K. C. Nicolaou, N. Watanabe, J. Li, J. Pastor and N. Winssinger, *Angew. Chem.*, 1998, **110**, 1636.
22 S. M. Sternson and S. L. Schreiber, *Tetrahedron Lett.*, 1998, **39**, 7451.
23 A. Tuchinsky and U. Zehavi, *React. Funct. Polym.*, 1999, **39**, 147.
24 R. Sreekumar, Y. Q. Pi, X. P. Huang and J. W. Walker, *Bioorg. Med. Chem. Lett.*, 1997, **7**, 341.
25 R. Reinhard and B. F. Schmidt, *J. Org. Chem.*, 1998, **63**, 2434; R. Reinhard and B. F. Schmidt, *J. Org. Chem.*, 1998, **63**, 3152.
26 L. Peng, J. Wirz and M. Goeldner, *Tetrahedron Lett.*, 1997, **38**, 2961.
27 D. Gravel, R. Giasson, D. Blanchet, R. W. Yip and D. K. Sharma, *Can. J. Chem.*, 1991, **69**, 1193.
28 R. W. Yip, Y. X. Wen, D. Gravel, R. Giasson and D. K. Sharma, *J. Phys. Chem.*, 1991, **95**, 6078.
29 J. E. T. Corrie, *J. Chem. Soc., Perkin Trans. 1*, 1993, 2161.
30 J. M. Bakke and H.-J. Engan, *Acta Chem. Scand. Ser. B*, 1978, **32**, 230.
31 W. K. Wong, H. Schupp and W. Schnabel, *Macromolecules*, 1989, **22**, 2176.
32 S. Schneider, M. Fink, R. Bug and H. Schupp, *J. Photochem. Photobiol., A*, 1991, **55**, 329.
33 A. Barth, J. E. T. Corrie, M. J. Gradwell, Y. Maeda, W. Mäntele, T. Meier and D. R. Trentham, *J. Am. Chem. Soc.*, 1997, **119**, 4149.
34 J. E. T. Corrie, J. Baker, E. M. Ostap, D. D. Thomas and D. R. Trentham, *J. Photochem. Photobiol., A*, 1998, **115**, 49.
35 R. W. Yip and D. K. Sharma, *Res. Chem. Intermed.*, 1989, **11**, 109.
36 S. Kuberski and J. Gębicki, *J. Mol. Struct.*, 1992, **275**, 105.
37 M. Carcelli, P. Pelagatti and C. Viappiani, *Isr. J. Chem.*, 1998, **38**, 213.
38 G. Wettermark, *J. Phys. Chem.*, 1962, **66**, 2560.
39 J. Michalak, T. Bally and J. Gębicki, *Radiat. Phys. Chem.*, 1995, **45**, 749.
40 I. R. Dunkin, J. Gębicki, M. Kiszka and D. Sanín-Leira, *Spectrochim. Acta, Part A*, 1997, **53**, 2553.
41 D. Lin-Vien, N. B. Colthup, W. G. Fateley and J. G. Grasselli, *The Handbook of Infrared and Raman Characteristic Frequencies of Organic Molecules*, Academic Press, Boston, 1991.
42 J. Hamer and A. Macaluso, *Chem. Rev.*, 1964, **64**, 473.
43 V. Baliah and V. C. Nair, *J. Indian Chem. Soc.*, 1989, **66**, 42.
44 A. P. Scott and L. Radom, *J. Phys. Chem. A*, 1996, **100**, 16502.
45 For an up-to-date discussion of the merits of DFT computations, including a comparison of methods for computing IR transitions, see W. Koch and M. C. Holthausen, *A Chemist's Guide to Density Functional Theory*, Wiley-VCH, Weinheim, 2000.
46 See, for example P. G. Sammes, *Tetrahedron*, 1976, **32**, 405; R. Haag, J. Wirz and P. J. Wagner, *Helv. Chim. Acta*, 1977, **60**, 2595; J. C. Scaiano, *Acc. Chem. Res.*, 1982, **15**, 252; P. J. Wagner, *Acc. Chem. Res.*, 1989, **22**, 83.
47 D. Seebach, H.-O. Kalinowski, B. Bastani, G. Crass, H. Daum, H. Dörr, N. P. DuPreez, V. Ehrig, W. Langer, C. Nüssler, H.-A. Oei and M. Schmidt, *Helv. Chim. Acta*, 1977, **60**, 301.
48 I. R. Dunkin and J. G. MacDonald, *J. Chem. Soc., Perkin Trans. 2*, 1984, 2079.
49 R. Withnall, I. R. Dunkin and R. Snaith, *J. Chem. Soc., Perkin Trans. 2*, 1994, 1973.
50 I. R. Dunkin, *Matrix-Isolation Techniques: A Practical Approach*, Oxford University Press, Oxford, 1998.
51 M. J. Frisch, G. W. Trucks, H. B. Schlegel, G. E. Scuseria, M. A. Robb, J. R. Cheeseman, V. G. Zakrzewski, J. A. Montgomery, Jr., R. E. Stratmann, J. C. Burant, S. Dapprich, J. M. Millam, A. D. Daniels, K. N. Kudin, M. C. Strain, O. Farkas, J. Tomasi, V. Barone, M. Cossi, R. Cammi, B. Mennucci, C. Pomelli, C. Adamo, S. Clifford, J. Ochterski, G. A. Petersson, P. Y. Ayala, Q. Cui, K. Morokuma, D. K. Malick, A. D. Rabuck, K. Raghavachari, J. B. Foresman, J. Cioslowski, J. V. Ortiz, A. G. Baboul, B. B. Stefanov, G. Liu, A. Liashenko, P. Piskorz, I. Komaromi, R. Gomperts, R. L. Martin, D. J. Fox, T. Keith, M. A. Al-Laham C. Y. Peng, A. Nanayakkara, M. Challacombe, P. M. W. Gill, B. Johnson, W. Chen, M. W. Wong, J. L. Andres, C. Gonzalez, M. Head-Gordon, E. S. Replogle and J. A. Pople, Gaussian 98W (Revision A.9), Gaussian, Inc., Pittsburgh, 1998.
52 C. Peng and H. B. Schlegel, *Isr. J. Chem.*, 1994, **33**, 449.
53 C. Peng, P. Y. Ayala, H. B. Schlegel and M. J. Frisch, *J. Comput. Chem.*, 1996, **17**, 49.